

Data-driven Discovery for Robust Optimization of Semiconductor Nanowire Lasers

Stephen A Church,^{*,†} Francesco Vitale,[‡] Aswani Gopakumar,[¶] Nikita Gagrani,[¶]
Yunyan Zhang,[§] Nian Jiang,^{||} Hark Hoe Tan,[¶] Chennupati Jagadish,[¶] Huiyun
Liu,[⊥] Hannah Joyce,^{||} Carsten Ronning,[‡] and Patrick Parkinson^{*,†}

[†]*Department of Physics and Astronomy and The Photon Science Institute, The University
of Manchester, M13 9PL, United Kingdom*

[‡]*Institute for Solid State Physics, Friedrich Schiller University Jena, Max-Wien-Platz 1,
07743 Jena, Germany*

[¶]*Department of Electronic Materials Engineering, Research School of Physics, The
Australian National University, Canberra, ACT, 2601 Australia*

[§]*College of Integrated Circuits, Zhejiang University, Hangzhou, Zhejiang 311200, China*

^{||}*Department of Engineering, University of Cambridge, CB2 1PZ, United Kingdom*

[⊥]*Department of Electronic and Electrical Engineering, University College London, WC1E
7JE, United Kingdom*

E-mail: stephen.church@manchester.ac.uk; patrick.parkinson@manchester.ac.uk

Abstract

Active wavelength-scale optoelectronic components are widely used in photonic integrated circuitry, however coherent sources of light – namely optical lasers – remain the most challenging component to integrate. Semiconductor nanowire lasers represent a flexible class of light source where each nanowire is both gain material and cavity; however, strong coupling between these properties and the performance leads

to inhomogeneity across the population. While this has been studied and optimized for individual material systems, no architecture-wide insight is available. Here, nine nanowire laser material systems are studied and compared using 55,516 nanowire lasers to provide statistically robust insight into performance. These results demonstrate that, while it may be important to optimise internal quantum efficiency for certain materials, cavity effects are always critical. Our study provides a roadmap to optimize the performance of nanowire lasers made from any material: this can be achieved by ensuring a narrow spread of lengths and end-facet reflectivities.

The miniaturisation of opto-electronic devices is an area of rapid development across multiple research fields.¹⁻³ In its simplest form this involves the development of devices at the centi- and millimeter-scale, enabling previously bulky apparatus to become light-weight and portable, facilitating accurate field-based testing, with applications including quality control⁴ and medical screening.⁵ Further miniaturisation, to the micron-scale, has yielded significant advancements in commercial technology. This includes micro-LEDs,⁶ which form the foundation of ultra-efficient, high-resolution and wide colour-gamut display technologies,⁷ enabling commercial virtual and augmented reality headsets.³

Nanoscale coherent light sources are widely sought after as biological probes,^{8,9} sensors, in quantum applications^{10,11} and most often as active components for photonic integrated circuitry^{2,12-14} that integrate micron-scale light sources, waveguides and detectors at high densities to perform light-based computing processes.¹⁵ A wide range of architectures have been proposed as solutions, spanning off-chip coupling, flip-chip integration and hetero-epitaxial growth.¹⁶⁻¹⁸ However, repeatable, high-density and high-yield laser sources are rare. Of particular concern is the strong coupling between material quality, cavity design and performance, which mean that small variations in defect density, surface passivation, hetero-junction parameters and geometry lead to significant effects for performance.^{6,20,21}

Nanoscale lasers based on semiconductor nanowires (NWs) have long been proposed as coherent light sources that are well suited to integration;²²⁻²⁶ these provide diverse emission

properties, such as wavelength, pulse duration and modal structure, arising from the wide choice of material system, while being united in their fundamental operating principle of the nanowire forming a monolithic cavity and gain material. These NW lasers (NWLs) typically have widths of 100's nm and lengths up to 10's μm . High refractive indices result in strong optical confinement, and the narrow NW widths often lead to a deterministic relationship between cavity, material and performance properties that necessitate optimization of each parameter.²⁷ The variety of material systems has led to a divergence in this optimization and development, and to-date high quality systems have been demonstrated in chalcogenides,^{28,29} nitrides,^{30,31} perovskites,^{32,33} metal oxides^{34,35} and III-Vs.^{4,36,37} This range of systems provides significant advantages for selecting lasing wavelength, for high-speed operation³⁹ or providing specific non-linear properties,⁴⁰ however it has led to a fragmentation in characterization methods⁴¹ resulting in a lack of robust inter-class comparison. This is exacerbated by the differences between growth mechanisms (for instance, selective-area growth⁴² versus vapour-liquid-solid⁴³) and the inclusion of plasmonic³⁹ or dielectric-enhanced³⁴ emission.

Tight control of the device fabrication is therefore required to minimise variation in performance and to maximise the useful yield. This is a crucial step towards commercialisation of these miniature technologies, with yield requirements as high as, for example, 99.9999% in the microLED industry.⁴⁴ Whilst an increasing number of reports now provide statistically robust intra-type results,^{27,36,45,46} comparison between nanowire types is rare, causing two significant roadblocks to further nanowire laser development: the lack of a common measurement methodology²⁷ to produce comparable data, and the resultant impossibility of obtaining globally meaningful insight from specific studies.

In this work, we use the principles of experimental data-led discovery⁴⁷ to generate an experimental understanding of nanowire laser (NWL) performance. This involves studying nine different NWL designs with nine independent automated experiments,³⁶ including bright field optical imaging, fluence-dependent photoluminescence, time-correlated single photon counting (TCSPC) and interferometry, with 55,516 NWLs investigated in total. The

approach enables the best-in-class NWs to be identified, a statistically rigorous comparison of the performance of each NW type and the identification of global trends and important factors that are independent of the NW design.

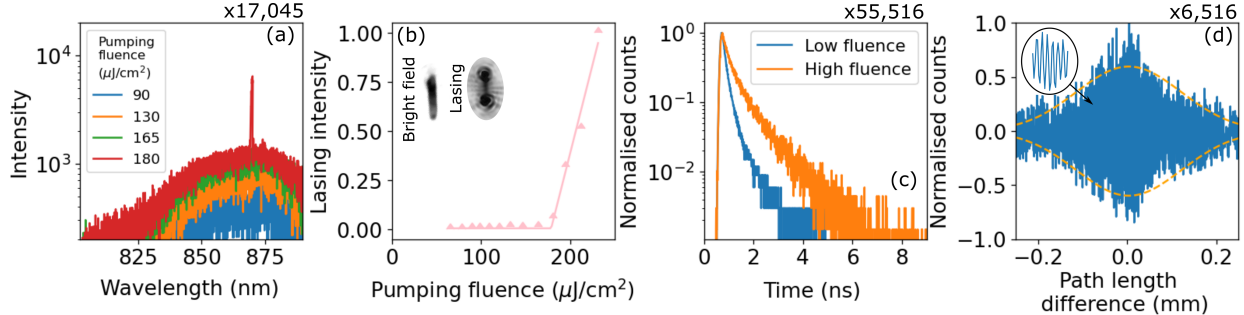


Figure 1: An example of the measurements taken from one individual InP NW, with numbers in the titles indicating the total number of NWs each measurement was performed for. (a) Power dependent photoluminescence spectra showing the emergence of a single lasing mode above a threshold fluence. (b) The light-in-light-out curve for this NW. The insets show the bright field and lasing emission images. (c) TCSPC PL decays measured below lasing threshold at low fluence and high fluence. (d) Interferogram of the lasing emission, with a Gaussian envelope, used to extract the coherence length.

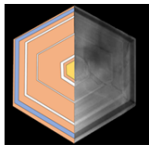
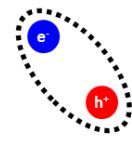
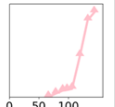
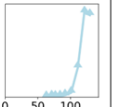
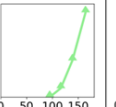
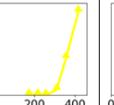
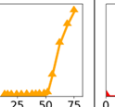
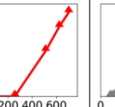
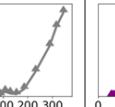
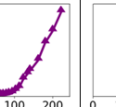
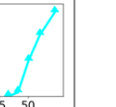
A summary of the measurements performed on one individual InP nanowire are displayed in Figure 1. Power-dependent photoluminescence measurements exhibit a broad spontaneous emission peak at all pumping fluences, along with a narrow-band emission peak, above a threshold fluence, that is attributed to stimulated emission. The threshold is identified by analysing the light-in-light-out (LILO) curves of the excitation fluence vs the intensity of the emission, an example of which is shown in Figure 1(b). These curves are produced and processed using an established algorithm.³⁶ In short, the emission intensity increases approximately linearly above lasing threshold, and a straight line was fit to this data and extrapolated to $y = 0$ in order to estimate a lasing threshold fluence. Using this approach, the threshold for this NW was determined to be $(178 \pm 3) \mu\text{J cm}^{-2}$.

TCSPC decays measured below the lasing threshold for the example NW are shown in Figure 1(c). For this NW, the $1/e$ decay time was 0.17 ns at low fluence, increasing to 0.30 ns at higher fluences. We attribute this fast decay to non-radiative recombination at point defects in the InP crystal structure. This is in agreement with earlier studies, where

InP NWs, and SAG grown NWs, have shown low surface recombination velocities.⁴⁸

Finally, a time-gated interferogram of the lasing emission above threshold was measured, shown in Figure 1(d), using an approach detailed in ref.³⁶ A modulation envelope can clearly be observed in the data. The laser coherence length of the radiation was defined as the full width at half maximum (FWHM) of this envelope, which was found to be 0.28 mm for this NW. This coherence length is several orders of magnitude longer than the NW length (6 μm). This is typical behaviour for the strong waveguides that are formed by NWs,⁴⁹ and is comparable to previous measurements on alternative materials.³⁶ Using this result, the end-facet reflectivity was calculated to be using a previously detailed approach.⁵⁰ This reflectivity is enhanced beyond the simple Fresnel reflection coefficient for this material (30%),⁵¹ which is indicative of a high quality cavity.⁴⁹

Table 1: The nine types of nanowires investigated in this study. Bright field optical images are shown for an example NW of each type, along with lasing emission images of the same NWs, demonstrating that the majority of the lasing emission is from the end facets. Emission imaging for GaN and ZnO was not possible due to a lack of sensitivity of the imaging camera to UV light. The lowest threshold NW has been identified for each NW type, and the light-in-light-out curves for each are shown, along with the threshold fluence. The heterostructure image has been adapted from ref.⁵⁰

	"Bulk" 			Heterostructure 			Excitonic 		
10 μm 	InP	GaAs	ZnGaAs	AlGaAs/ GaAs	GaAsP/ GaAs - 1	GaAsP/ GaAs - 2	CdS	GaN	ZnO
Bright field									
Lasing								N/A	N/A
Best-in-type intensity vs fluence	113 $\mu\text{J}/\text{cm}^2$ 	101 $\mu\text{J}/\text{cm}^2$ 	123 $\mu\text{J}/\text{cm}^2$ 	303 $\mu\text{J}/\text{cm}^2$ 	51 $\mu\text{J}/\text{cm}^2$ 	283 $\mu\text{J}/\text{cm}^2$ 	164 $\mu\text{J}/\text{cm}^2$ 	104 $\mu\text{J}/\text{cm}^2$ 	35 $\mu\text{J}/\text{cm}^2$ 

A large, multidimensional dataset was generated by performing the measurements in Figure 1 for NWs of different architectures, which are summarized in Table 1. This includes “bulk” selective-area-grown InP,³ vapour-liquid-solid grown surface-passivated GaAs,⁴ Zn-doped GaAs,¹ core-shell quantum well (QW) heterostructures AlGaAs/GaAs⁵ and GaAsP/GaAs, which has 2 growth batches - 1 and - 2.^{50,55} Also included are NWs which demonstrate excitonic emission at room temperature due to large exciton binding energies: CdS,⁸ GaN,⁵⁷ and ZnO.^{10,59} Table 1 shows an exemplary bright field optical image for each type of NWL. For comparison, images of the spatial emission profile above lasing threshold for the same wires are also shown in Table 1. In this regime, the majority of the light couples out of the end facets of the NW Fabry-Perot cavity. Each end facet acts as an independent, coherent, point source of light and interference fringes between these two sources are observed in the far field.⁴

Using this dataset, it is trivial to identify the best-in-type lasers by assessing the lasing thresholds. The LILO curves for these champion NWs are shown in Table 1. The lowest observed threshold was $(35 \pm 1) \mu\text{J cm}^{-2}$ from a ZnO NWL. This is consistent with measurements using similar excitation conditions on NWs of comparable size and geometry.⁶⁰ However, this is two orders of magnitude higher than the lowest-reported thresholds in the literature,⁶¹ highlighting the sensitivity of this measurement to the experimental conditions and NW size.

The GaAsP/GaAs - 1 NWs also perform favourably, with a lowest threshold of $(51 \pm 1) \mu\text{J cm}^{-2}$, which is similar to the best in the literature for this material.^{50,55} However, the alternative growth batch GaAsP/GaAs - 2, has a champion threshold which is more than five times higher - emphasising the impact that tuned growth conditions can have on performance. Despite this, it is interesting to note that the best-in-class thresholds are of a similar order of magnitude ($100 \mu\text{J cm}^{-2}$) for most types. This implies that, for the best-performing NWs, the functional performance in the pulsed excitation regime may be limited by the same effects, independent of the design and material used. This is possibly

because the excitation and lasing occurs on timescales faster than many material-dependent carrier recombination processes.⁵⁰

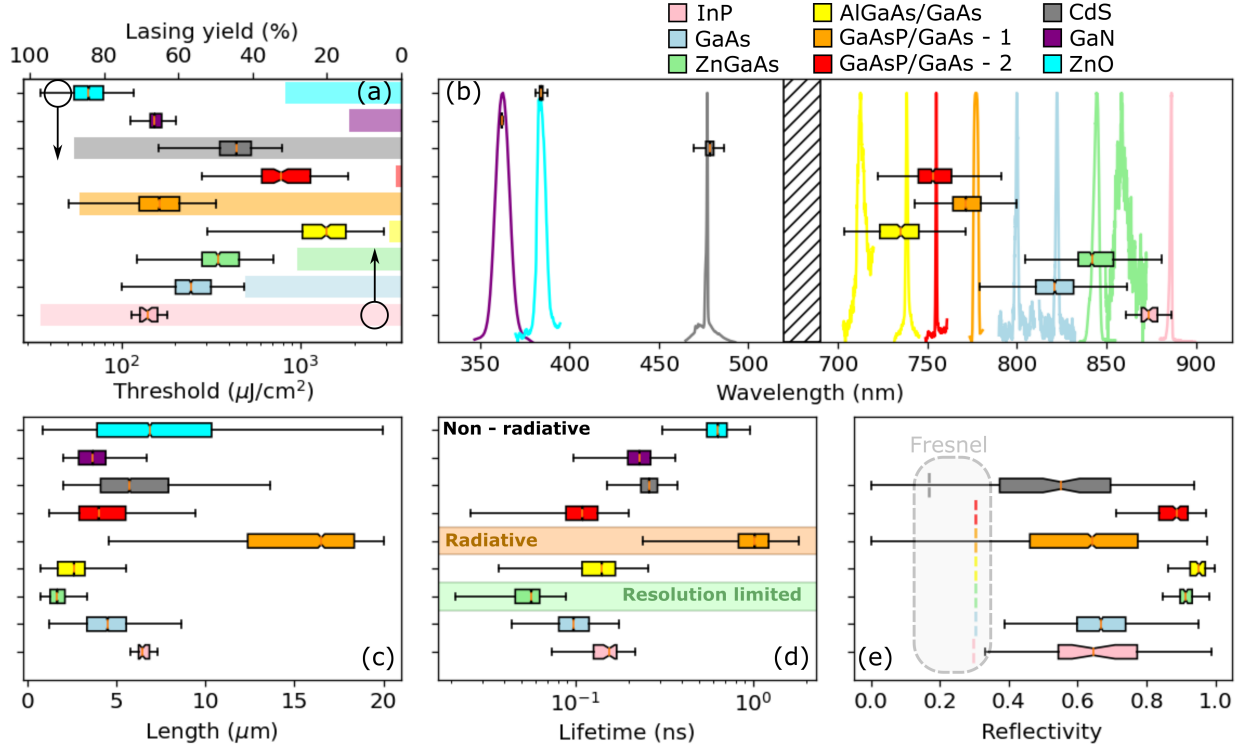


Figure 2: Intra-type statistics. (a) The lasing threshold fluence (box plot) with lasing yield (bar chart) for each NWL type. (b) The peak wavelength of the fundamental lasing mode at threshold. The lasing spectra of selected NWLs are also shown. (c) Cavity length for all NWs measured from bright field imaging, accurate to $\approx 0.5 \mu\text{m}$. (d) The carrier recombination lifetime measured at low fluence, the coloured background indicate dominated radiative (GaAsP/GaAs - 1) and non-radiative decays (white background), and those which are resolution limited (green background). (e) The end-facet reflectivity calculated from the coherence length, the dashed lines are the calculated Fresnel reflection coefficients for a planar surface, assuming the refractive index of InP, GaAs and CdS.⁵¹ Reflectivity values were not obtained for GaN or ZnO NWLs due to a lack of sensitivity to UV emission for this technique.

The data-led approach enables our study to extend from simple best-in-class measurements (Figure 1), through providing robust intra-class measurements of single NWL types (Table 1), to understanding global (inter-class) NWL architecture effects. The lasing threshold fluence and the lasing yield (the percentage of NWs with a lasing threshold below their damage threshold) are displayed in Figure 2(a). The lowest median threshold is seen in ZnO, with $65 \mu\text{J cm}^{-2}$. Furthermore, the GaAsP/GaAs - 1 NWLs, despite having one of the lowest

threshold champion devices, demonstrate a large variation in the threshold, such that the median is $163 \mu\text{J cm}^{-2}$, and close to that of the other NWs. In contrast, the lasing yield for GaAsP/GaAs - 1 NWs is one of the highest available (86.5%), and is significantly higher than the yield of ZnO NWs (31%). Clearly the interplay between yield and threshold is not straightforward. Reporting best-in-class values for NWs is at best ambiguous, and at worst misleading for inter-class comparison.

The largest median thresholds and threshold variation are seen in the AlGaAs/GaAs and GaAsP/GaAs - 2 core/shell QW NWs, which have thresholds between 1000 and $2000 \mu\text{J cm}^{-2}$. These NWs also have the lowest yields, just 2 and 3%; this is likely because the lasing thresholds are close to the damage threshold of the NWs. Careful NW heterostructure design is essential to ensure that the QWs overlap well with the transverse lasing modes, and this must be maintained across a population through growth optimisation.

The distribution of the lasing wavelength for each class is shown in Figure 2(b). These wavelengths depend upon both the laser gain spectrum and the cavity.⁴ The wavelength variation in each class can be as high as 100 nm: as a result, the full NW population has continuous wavelength coverage across the spectral window between 700 and 880 nm. While this variability presents the most significant obstacle to scale-up, this does provide a means of effectively tuning the wavelength by selecting a NW with the desired properties.⁶² To demonstrate this coverage, the lasing spectra for 12 NWs are shown in Figure 2(b); these NWs have been chosen to change the lasing wavelength by 20 nm across the 700 nm-880 nm range, although it is possible to select NWs based on wavelength with nm-level precision, due to the size of the NW population. This type of data-driven screening is useful as a way to target ideal devices for transfer printing into photonic integrated circuits.⁴⁶

The distribution of NW lengths are shown in Figure 2(c). The lengths vary between $1 \mu\text{m}$, which is the resolution of the optical imaging, and $20 \mu\text{m}$. These distributions offer a simple assessment of the uniformity of the growth dynamics and the NW transfer process.⁶³ In this case, the InP NWs stand out as being the most uniform, with an interquartile range

(IQR) of 9%; as the only selective-area grown nanowires, this uniformity is a demonstration of the advantage of catalyst-free growth for geometrical homogeneity. The GaAsP/GaAs - 1 length distribution is also distinctive, as this has the largest median length of 16.4 μm , which is more than 10 μm longer than the other heterostructure NW types. This is a strong indication of the importance of the NW length on the performance: Figure 2(a) shows that these NWs also have an order of magnitude lower threshold than the other heterostructures, including those of the same material, which is due to the larger volume of gain material for longer NWs.⁶

Figure 2(d) shows the distributions for the below-threshold photoluminescence lifetime measured from TCSPC decays. This metric is intrinsic to each material system, and is a combination of the radiative and non-radiative recombination rates. The InP, GaAs, AlGaAs/GaAs, GaAsP/GaAs - 2, CdS, GaN and ZnO NWs all exhibit lifetimes that are short when compared with radiative lifetimes of comparable materials,^{64–69} with median values between 100 and 640 ps, and are therefore dominated by non-radiative recombination effects. However, the impact of the surface is likely to be reduced for these samples: this is evidenced by low surface recombination velocities for InP NWs,⁴⁸ the passivation of the surface for the GaAs, AlGaAs/GaAs and GaAsP/GaAs NWs and comparable measurements for layers of CdS, GaN and ZnO.^{70–72} Each class shows pumping fluence-dependent TCSPC measurements similar to Figure 1(c), so we associate this lifetime with non-radiative recombination of point defects in the NWs. The lifetime therefore provides a proxy of the material quality: a higher defect density will shorten the recombination lifetime. The Zn-doped GaAs NWs show the fastest mean lifetime of 57 ps, however this measurement is limited by the time resolution, and is due to rapid recombination, with a previously measured lifetime of 3–6 ps.^{1,73}

In contrast, GaAsP/GaAs - 1 NWs show the longest median recombination lifetime of 1 ns. This NWL batch has been previously studied,³⁶ where it was established that the recombination efficiency is around 39%, meaning that the rates of non-radiative and

radiative recombination are comparable. The median radiative lifetime is therefore 2.5 ns, and the median non-radiative lifetime is 1.6 ns. This suggests that the material quality of this sample is improved, in particular in comparison to GaAsP/GaAs - 2, such that the non-radiative recombination rate has been reduced by around an order of magnitude.

The end-facet reflectivity was calculated from measurements of the coherence length⁵⁰ as shown in Figure 1(d), and the distributions are shown in Figure 2(e). The vast majority of NWs have reflectivities that are enhanced above the Fresnel reflection factors for planar surfaces. This is consistent with previous measurements of a single NW class^{36,50} and experimentally verifies the theoretical predictions that have underpinned the use of the NW architecture for two decades.⁴⁹ The InP, GaAs, GaAsP/GaAs - 1 and CdS NWs show low median reflectivities around 0.6 and IQRs up to 0.31. This large degree of variation may be associated with differences in NW width - and thus changes in the waveguiding properties:⁴⁹ irregular morphology at the end facets, either due to the NW transfer procedure,⁶³ or from an abundance of lattice defects in this region,⁷⁴ may also play a role. The other NWs, Zn:GaAs, AlGaAs/GaAs and GaAsP/GaAs - 2, have high median reflectivities between 0.89 and 0.91 and IQRs up to 0.08. While statistically significant, these findings are likely a result of selection bias in the measurements due to the low yield of these NWs. Due to the nature of the measurement, reflectivities can only be determined for lasing NWs: thus, high material quality NWs can operate with poor cavities, while low material quality (poor IQE) NWs require a high quality cavity to show lasing below their damage threshold.

Whilst analysing each parameter distribution in isolation can provide useful information regarding inhomogeneity in each type of NW, a key benefit of the holistic high-throughput approach is the ability to directly compare the distributions of different parameters for the same NWs and isolate correlations to investigate physical phenomena. In particular, the parameters that are most important in controlling the lasing threshold can be determined. This is facilitated by the large population sizes in this study: for example, if a correlative analysis is attempted in a small data study, with approximately 100 NWs, an important

correlation between two parameters will be obscured by the significant variation in the other parameters, as suggested by the boxplots in Figure 2.

To investigate the most important factors that influence the lasing threshold, the datasets were normalised by subtracting the median and dividing by the standard deviation of each distribution for each NW type. This data was then grouped into 3 classes, as defined by Table 1: excitonic, “bulk” and heterostructure. The linear correlation parameters between the threshold and other key parameters were calculated for each group. This includes material (from PL and lifetime measurements), cavity (dimensions and reflectivity) and performance (lasing wavelength) properties for each group, shown in Fig. 3(a). This provides an at-a-glance means of assessing the performance, averaging over any inter-type variation in NW growths, and enables global trends to be observed that are related to the underlying physics and performance of NWs.

These results elucidate the importance of the laser cavity on all classes of NWs. In all cases, the NW length has a significant negative correlation with threshold, which confirms the conclusions from Figure 2 in a statistically rigorous manner. This dictates a clear route towards optimising the threshold of all types of NWs: minimise the length variation between each NW. A similar effect is also observed for increasing the width of “bulk” and excitonic NWs, which is compounded by an additional increase in the optical confinement factor. However, no width correlation is observed for heterostructure samples: this suggests that the optical gain is decoupled from the NW width and confinement factor, instead depending on the QW width and QW-lasing mode overlap.⁵

The strength of the length correlation reduces from excitonic ($r = -0.17$), to “bulk” ($r = -0.11$) and to heterostructure ($r = -0.05$) lasers. This suggests that the length has different degree of impact on the threshold for different NW classes. A possible explanation for this is due to differences in distributed losses between the NW classes, which would partially counter-balance the increased gain. For example, for heterostructure NWs, the overgrowth of the shells can lead to distortions in the NW cross-section shape and consequently enhance

the optical losses.⁷⁴

The cavity reflectivity also plays a crucial role in the performance, which shows a negative correlation with threshold for “bulk” and heterostructure lasers, indicating that a higher reflectivity reduces the optical losses and, thus, the threshold. No trend is observed for the excitonic NWs, although this may be due to a small sample size (90 wires in total). Another route to reduce variation in NWL performance is therefore to optimise the end facets, either by optimising the NW transfer⁶³ or standardising the NW width during growth.⁴⁹

In contrast, the material properties of the NWs do not show consistent correlations with threshold. The PL FWHM, an often-used measure of the inhomogeneity in the material,⁶ has no statistically significant impact on the threshold. The carrier lifetime also shows no correlation for “bulk” NWs, which suggests that, despite the variation in lifetime shown in Fig. 2(d), there is little significant change in the quantum efficiency of these classes across their populations. In contrast, the heterostructure and excitonic lasers show a negative correlation between lifetime and threshold. This correlation has been discussed in detail previously,³⁶ and is attributed to a variation in the non-radiative recombination rate (and quantum efficiency) which is related to a change in defect density within the gain medium. For these samples, there remains scope to improve the lasing performance by improving the IQE of the active layer by optimising the growth conditions to reduce the defect density.

The PL peak energy in “bulk” and heterostructure NWs show a positive correlation with threshold. The mechanism for the energy variation is related to composition, strain or heterostructure fluctuations, depending on the sample, and this also leads to shifts in the laser gain spectrum. These correlations are a consequence of the strong negative correlations between lasing wavelength and threshold which have been previously attributed to reabsorption¹ and band-filling effects.³⁶ Interestingly, the excitonic devices show an opposite negative correlation between PL peak energy and threshold. This is consistent with previous studies that demonstrate the importance of strong exciton binding to achieve lasing:⁷⁵ NWs with more strongly bound excitons are more likely to have a lower lasing threshold.

This is despite the lasing action being sustained by an electron-hole plasma which forms at high fluences.⁷⁶

The wavelength correlation for each NW class shows the same effects to a different degree. The excitonic devices, shown in Figure 3(b), have minimal reabsorption since the peak of the gain spectrum lies in the material bandgap, the 3D density of states and excitonic recombination also reduces the impact of band-filling and so the correlation between wavelength and threshold is the lowest of the three classes. The “bulk” class (Fig. 3(c)) has more reabsorption, and so the correlation is increased. Finally, the heterostructure NWs (Fig. 3(d)) exhibit reabsorption into core and cap layers, and will exhibit more band-filling due to a reduced 2D density of states³⁶ and thus have the highest observed correlation.

In summary, we have demonstrated a data-driven experimental approach to study large numbers of micron-scale opto-electronic devices. We have applied this to investigate the properties of 55,516 individual NWs with nine different designs and have extracted parameters that describe how the gain medium, lasing cavity and performance vary across the population. We have shown how the approach can be used to effectively screen for the best-in-class devices and we have quantified the statistical distribution of each parameter and used this to compare the properties of different NW types in a statistically robust manner. Through a correlative analysis, it was determined that the properties of the laser cavity are consistently a driving factor in the performance of NWs and this elucidates a route towards achieving homogeneous performance across a population of any type of NWs: by optimising the NW length and end-facet reflectivity.

Acknowledgement

Supporting information is available for this paper, which includes the growth details for each type of nanowire. This can be found at DOI: ????.

This work was funded by UKRI under grants MR/T021519/1, EP/V036343/1 and

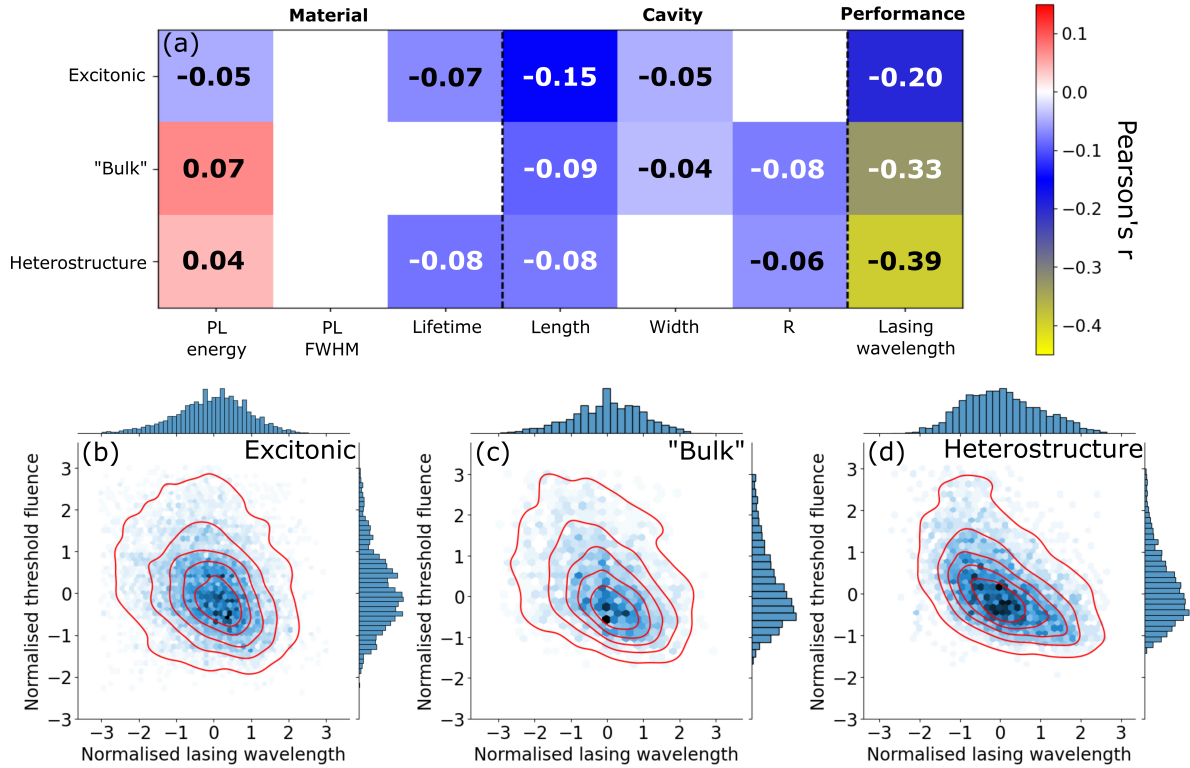


Figure 3: A correlative analysis of the lasing threshold pumping fluence. (a) Statistically significant (with a p -value < 0.05) Pearson's linear correlation coefficients between normalised NW parameters and the lasing pumping threshold, grouped into three NW classes. White indicates parameters where $p > 0.05$ and so there is no statistically significant correlation, whereas red and blue are significant positive and negative correlations respectively. Yellow is representative of a strong negative correlation with $r < -0.2$. GaAsP/GaAs - 2 and AlGaAs/GaAs NWs are removed from the reflectivity analysis due to selection bias in the distributions. GaN and ZnO NWs are also removed from the reflectivity analysis due to a lack of sensitivity to UV light. Zn:GaAs NWs are removed from the lifetime analysis due to experimental resolution issues. Normalised 2D histograms are also shown, which display the relationship between normalised lasing wavelength and threshold for each class: (b) excitonic, (c) "bulk" and (d) heterostructure.

EP/W002302/1, by the Deutsche Forschungsgemeinschaft within the frame of the collaborative research center CRC 1375 (project C5), by the Australian Research Council, the Australian National Fabrication Facility ACT node, as well as China special Grant (134000-E62201ZJ); Zhejiang Provincial Natural Science Foundation of China (Z24F040009), Zhejiang University Education Foundation Qizhen Scholar Foundation (K20240015), and CMOS Special Program of Zhejiang University (04010000-K2A033208). Research data supporting this publication will be made available at DOI: (DOI to be provide in due course), and the code to perform the analysis will be made available at DOI: (DOI to be provide in due course), and on github: (URL to be provide in due course).

CRediT author statement: **Stephen Church**: Formal analysis, Investigation, Methodology, Software, Visualisation, Writing - original draft. **Francesco Vitale, Aswani Gopakumar, Nikita Gagrani, Yunyan Zhang, Nian Jiang, Hark Hoe Tan, Chennupati Jagadish, Huiyun Liu, Hannah Joyce and Carsten Ronning**: Resources, Writing - review and editing. **Patrick Parkinson**: Conceptualization, Data curation, Funding acquisition, Methodology, Software, Supervision, Writing - review and editing.

References

- (1) Park, S. I. et al. Soft, stretchable, fully implantable miniaturized optoelectronic systems for wireless optogenetics. *Nature Biotechnology* **2015**, *33*, 1280–1286.
- (2) Zhang, J. et al. III-V-on-Si photonic integrated circuits realized using micro-transfer-printing. *APL Photonics* **2019**, *4*, 110803.
- (3) Xiong, J.; Hsiang, E.-L.; He, Z.; Zhan, T.; Wu, S.-T. Augmented reality and virtual reality displays: emerging technologies and future perspectives. *Light: Science & Applications* **2021**, *10*, 216.

- (4) Li, Z.; Suslick, K. S. Portable Optoelectronic Nose for Monitoring Meat Freshness. *ACS Sensors* **2016**, *1*, 1330–1335.
- (5) Bansal, A. K.; Hou, S.; Kulyk, O.; Bowman, E. M.; Samuel, I. D. W. Wearable Organic Optoelectronic Sensors for Medicine. *Advanced Materials* **2015**, *27*, 7638–7644.
- (6) Wu, T.; Sher, C.-W.; Lin, Y.; Lee, C.-F.; Liang, S.; Lu, Y.; Huang Chen, S.-W.; Guo, W.; Kuo, H.-C.; Chen, Z. Mini-LED and Micro-LED: Promising Candidates for the Next Generation Display Technology. *Applied Sciences* **2018**, *8*, 1557.
- (7) Zhou, X.; Tian, P.; Sher, C.-W.; Wu, J.; Liu, H.; Liu, R.; Kuo, H.-C. Growth, transfer printing and colour conversion techniques towards full-colour micro-LED display. *Progress in Quantum Electronics* **2020**, *71*, 100263.
- (8) Fikouras, A. H.; Schubert, M.; Karl, M.; Kumar, J. D.; Powis, S. J.; Di Falco, A.; Gather, M. C. Non-obstructive intracellular nanolasers. *Nature Communications* **2018**, *9*, 4817.
- (9) Wu, X.; Chen, Q.; Xu, P.; Chen, Y. C.; Wu, B.; Coleman, R. M.; Tong, L.; Fan, X. Nanowire lasers as intracellular probes. *Nanoscale* **2018**, *10*, 9729–9735.
- (10) Pirandola, S. et al. Advances in quantum cryptography. *Advances in Optics and Photonics* **2020**, *12*, 1012.
- (11) Sutula, M.; Christen, I.; Bersin, E.; Walsh, M. P.; Chen, K. C.; Mallek, J.; Melville, A.; Titze, M.; Bielejec, E. S.; Hamilton, S.; Braje, D.; Dixon, P. B.; Englund, D. R. Large-scale optical characterization of solid-state quantum emitters. *Nature Materials* **2023**, *22*, 1338–1344.
- (12) Yang, J.; Tang, M.; Chen, S.; Liu, H. From past to future: on-chip laser sources for photonic integrated circuits. *Light: Science & Applications* **2023**, *12*, 1–3.

- (13) Sun, C. et al. Single-chip microprocessor that communicates directly using light. *Nature* **2015**, *528*, 534–538.
- (14) Wang, J.; Sciarrino, F.; Laing, A.; Thompson, M. G. Integrated photonic quantum technologies. *Nature Photonics* **2020**, *14*, 273–284.
- (15) Shastri, B. J.; Tait, A. N.; Ferreira de Lima, T.; Pernice, W. H. P.; Bhaskaran, H.; Wright, C. D.; Prucnal, P. R. Photonics for artificial intelligence and neuromorphic computing. *Nature Photonics* **2021**, *15*, 102–114.
- (16) Mayer, B.; Janker, L.; Loitsch, B.; Treu, J.; Kostenbader, T.; Lichtmannecker, S.; Reichert, T.; Morkötter, S.; Kaniber, M.; Abstreiter, G.; Gies, C.; Koblmüller, G.; Finley, J. J. Monolithically Integrated High- β Nanowire Lasers on Silicon. *Nano Letters* **2016**, *16*, 152–156.
- (17) Stettner, T.; Kostenbader, T.; Ruhstorfer, D.; Bissinger, J.; Riedl, H.; Kaniber, M.; Koblmüller, G.; Finley, J. J. Direct Coupling of Coherent Emission from Site-Selectively Grown III-V Nanowire Lasers into Proximal Silicon Waveguides. *ACS Photonics* **2017**, *4*, 2537–2543.
- (18) Schuster, F.; Kapraun, J.; Malheiros-Silveira, G. N.; Deshpande, S.; Chang-Hasnain, C. J. Site-Controlled Growth of Monolithic InGaAs/InP Quantum Well Nanopillar Lasers on Silicon. *Nano Letters* **2017**, *17*, 2697–2702.
- (6) Alanis, J. A.; Saxena, D.; Mokkaapati, S.; Jiang, N.; Peng, K.; Tang, X.; Fu, L.; Tan, H. H.; Jagadish, C.; Parkinson, P. Large-scale statistics for threshold optimization of optically pumped nanowire lasers. *Nano Letters* **2017**, *17*, 4860–4865.
- (20) Liu, M.; Yazdani, N.; Yarema, M.; Jansen, M.; Wood, V.; Sargent, E. H. Colloidal quantum dot electronics. *Nature Electronics* **2021**, *4*, 548–558.

- (21) Wang, H. et al. Towards optimal single-photon sources from polarized microcavities. *Nature Photonics* **2019**, *13*, 770–775.
- (22) Parkinson, P. *Physics and applications of semiconductor nanowire lasers*; Elsevier, 2021; Vol. 20; pp 389–438.
- (23) Eaton, S. W.; Fu, A.; Wong, A. B.; Ning, C.-Z. Z.; Yang, P. Semiconductor nanowire lasers. *Nature Reviews Materials* **2016**, *1*, 16028.
- (24) Couteau, C.; Larrue, A.; Wilhelm, C.; Soci, C. Nanowire Lasers. *Nanophotonics* **2015**, *4*, 90–107.
- (25) Ning, C. Z. Semiconductor nanolasers. *Physica Status Solidi (B) Basic Research* **2010**, *247*, 774–788.
- (26) Huang, Y.; Lieber, C. M. Integrated nanoscale electronics and optoelectronics: Exploring nanoscale science and technology through semiconductor nanowires. *Pure and Applied Chemistry* **2004**, *76*, 2051–2068.
- (27) Church, S. A.; Al-Abri, R.; Parkinson, P.; Saxena, D. Optical characterisation of nanowire lasers. *Progress in Quantum Electronics* **2022**, *85*, 100408.
- (28) Bao, Q.; Li, W.; Xu, P.; Zhang, M.; Dai, D.; Wang, P.; Guo, X.; Tong, L. On-chip single-mode CdS nanowire laser. *Light: Science and Applications* **2020**, *9*, 42.
- (29) Li, J.; Meng, C.; Liu, Y.; Wu, X.; Lu, Y.; Ye, Y.; Dai, L.; Tong, L.; Liu, X.; Yang, Q. Wavelength Tunable CdSe Nanowire Lasers Based on the Absorption-Emission-Absorption Process. *Advanced Materials* **2013**, *25*, 833–837.
- (30) Li, C.; Wright, J. B.; Liu, S.; Lu, P.; Figiel, J. J.; Leung, B.; Chow, W. W.; Brener, I.; Koleske, D. D.; Luk, T. S.; Feezell, D. F.; Brueck, S. R.; Wang, G. T. Nonpolar In-GaN/GaN Core-Shell Single Nanowire Lasers. *Nano Letters* **2017**, *17*, 1049–1055.

- (31) Li, K. H.; Liu, X.; Wang, Q.; Zhao, S.; Mi, Z. Ultralow-threshold electrically injected AlGa_N nanowire ultraviolet lasers on Si operating at low temperature. *Nature Nanotechnology* **2015**, *10*, 140–144.
- (32) Dong, H.; Zhang, C.; Liu, X.; Yao, J.; Zhao, Y. S. Materials chemistry and engineering in metal halide perovskite lasers. *Chemical Society Reviews* **2020**, *49*, 951–982.
- (33) Schlaus, A. P.; Spencer, M. S.; Miyata, K.; Liu, F.; Wang, X.; Datta, I.; Lipson, M.; Pan, A.; Zhu, X. Y. How lasing happens in CsPbBr₃ perovskite nanowires. *Nature Communications* **2019**, *10*, 265.
- (34) Sergent, S.; Takiguchi, M.; Tsuchizawa, T.; Taniyama, H.; Notomi, M. Low-Threshold Lasing up to 360 K in All-Dielectric Subwavelength-Nanowire Nanocavities. *ACS Photonics* **2020**, acsphotronics.0c00166.
- (35) Vanmaekelbergh, D.; Van Vugt, L. K. ZnO nanowire lasers. *Nanoscale* **2011**, *3*, 2783–2800.
- (36) Church, S. A.; Patel, N.; Al-Abri, R.; Al-Amairi, N.; Zhang, Y.; Liu, H.; Parkinson, P. Holistic Nanowire Laser Characterization as a Route to Optimal Design. *Advanced Optical Materials* **2023**, *11*, 2202476.
- (37) Tatebayashi, J.; Kako, S.; Ho, J.; Ota, Y.; Iwamoto, S.; Arakawa, Y. Room-temperature lasing in a single nanowire with quantum dots. *Nature Photonics* **2015**, *9*, 501–505.
- (4) Saxena, D.; Mokkaapati, S.; Parkinson, P.; Jiang, N.; Gao, Q.; Tan, H. H.; Jagadish, C. Optically Pumped Room-Temperature GaAs Nanowire Lasers. *Nature Photonics* **2013**, *7*, 963–968.
- (39) Sidiropoulos, T. P. H.; Röder, R.; Geburt, S.; Hess, O.; Maier, S. A.; Ronning, C.; Oulton, R. F. Ultrafast plasmonic nanowire lasers near the surface plasmon frequency. *Nature Physics* **2014**, *10*, 870–876.

- (40) Yi, R. et al. Self-frequency-conversion nanowire lasers. *Light: Science & Applications* **2022**, *11*, 1–9.
- (41) Zimmler, M. A.; Capasso, F.; Müller, S.; Ronning, C. Optically pumped nanowire lasers: invited review. *Semiconductor Science and Technology* **2010**, *25*, 024001.
- (42) Noborisaka, J.; Motohisa, J.; Fukui, T. Catalyst-free growth of GaAs nanowires by selective-area metalorganic vapor-phase epitaxy. *Applied Physics Letters* **2005**, *86*, 1–3.
- (43) Wagner, R. S.; Ellis, W. C. Vapor-liquid-solid mechanism of single crystal growth. *Applied Physics Letters* **1964**, *4*, 89–90.
- (44) Chen, Z.; Yan, S.; Danesh, C. MicroLED technologies and applications: characteristics, fabrication, progress, and challenges. *Journal of Physics D: Applied Physics* **2021**, *54*, 123001.
- (45) Wong, W. W.; Wang, N.; Esser, B. D.; Church, S. A.; Li, L.; Lockrey, M.; Aharonovich, I.; Parkinson, P.; Etheridge, J.; Jagadish, C.; Tan, H. H. Bottom-up, Chip-Scale Engineering of Low Threshold, Multi-Quantum-Well Microring Lasers. *ACS Nano* **2023**,
- (46) Jevtics, D.; McPhillimy, J.; Guilhabert, B.; Alanis, J. A.; Tan, H. H.; Jagadish, C.; Dawson, M. D.; Hurtado, A.; Parkinson, P.; Strain, M. J. Characterization, Selection, and Microassembly of Nanowire Laser Systems. *Nano Letters* **2020**, *20*, 1862–1868.
- (47) Merchant, A.; Batzner, S.; Schoenholz, S. S.; Aykol, M.; Cheon, G.; Cubuk, E. D. Scaling deep learning for materials discovery. *Nature* **2023**, *624*, 80–85.
- (48) Joyce, H. J.; Wong-Leung, J.; Yong, C.-K.; Docherty, C. J.; Paiman, S.; Gao, Q.; Tan, H. H.; Jagadish, C.; Lloyd-Hughes, J.; Herz, L. M.; Johnston, M. B. Ultralow

- Surface Recombination Velocity in InP Nanowires Probed by Terahertz Spectroscopy. *Nano Letters* **2012**, *12*, 5325–5330.
- (49) Maslov, A. V.; Ning, C. Z. Reflection of Guided Modes in a Semiconductor Nanowire Laser. *Applied Physics Letters* **2003**, *83*, 1237–1239.
- (50) Skalsky, S.; Zhang, Y.; Alanis, J. A.; Fonseka, H. A.; Sanchez, A. M.; Liu, H.; Parkinson, P. Heterostructure and Q-factor Engineering for Low-threshold and Persistent Nanowire Lasing. *Light: Science and Applications* **2020**, *9*, 43.
- (51) Adachi, S. Optical dispersion relations for GaP, GaAs, GaSb, InP, InAs, InSb, AlGaAs, and InGaAsP. *Journal of Applied Physics* **1989**, *66*, 6030–6040.
- (3) Gao, Q.; Saxena, D.; Wang, F.; Fu, L.; Mokkapati, S.; Guo, Y.; Li, L.; Wong-Leung, J.; Caroff, P.; Tan, H. H.; Jagadish, C. Selective-area epitaxy of pure wurtzite InP nanowires: High quantum efficiency and room-temperature lasing. *Nano Letters* **2014**, *14*, 5206–5211.
- (1) Alanis, J. A.; Lysevych, M.; Burgess, T.; Saxena, D.; Mokkapati, S.; Skalsky, S.; Tang, X.; Mitchell, P.; Walton, A. S.; Tan, H. H.; Jagadish, C.; Parkinson, P. Optical Study of p-Doping in GaAs Nanowires for Low-Threshold and High-Yield Lasing. *Nano Letters* **2019**, *19*, 362–368.
- (5) Saxena, D.; Jiang, N.; Yuan, X.; Mokkapati, S.; Guo, Y.; Tan, H. H.; Jagadish, C. Design and Room-Temperature Operation of GaAs/AlGaAs Multiple Quantum Well Nanowire Lasers. *Nano Letters* **2016**, *16*, 5080–5086.
- (55) Zhang, Y.; Saxena, D.; Aagesen, M.; Liu, H. Toward Electrically Driven Semiconductor Nanowire Lasers. *Nanotechnology* **2019**, *30*, 192002.
- (8) Geburt, S.; Thielmann, A.; Röder, R.; Borschel, C.; McDonnell, A.; Kozlik, M.;

- Kühnel, J.; Sunter, K. A.; Capasso, F.; Ronning, C. Low threshold room-temperature lasing of CdS nanowires. *Nanotechnology* **2012**, *23*, 365204.
- (57) Jiang, N.; Ghosh, S.; Frentrop, M.; Fairclough, S. M.; Loeto, K.; Kusch, G.; Oliver, R. A.; Joyce, H. J. Complications in silane-assisted GaN nanowire growth. *Nanoscale Advances* **2023**, *5*, 2610–2620.
- (10) Borchers, C.; Müller, S.; Stichtenoth, D.; Schwen, D.; Ronning, C. Catalyst-Nanostructure Interaction in the Growth of 1-D ZnO Nanostructures. *The Journal of Physical Chemistry B* **2006**, *110*, 1656–1660.
- (59) Vitale, F.; Repp, D.; Siefke, T.; Zeitner, U.; Peschel, U.; Pertsch, T.; Ronning, C. Tailoring nanowire lasing modes via coupling to metal gratings. *Applied Physics Letters* **2023**, *122*.
- (60) Röder, R.; Sidiropoulos, T. P.; Buschlinger, R.; Riediger, M.; Peschel, U.; Oulton, R. F.; Ronning, C. Mode Switching and Filtering in Nanowire Lasers. *Nano Letters* **2016**, *16*, 2878–2884.
- (61) Johnson, J. C.; Yan, H. Q.; Yang, P. D.; Saykally, R. J. Optical cavity effects in ZnO nanowire lasers and waveguides. *Journal of Physical Chemistry B* **2003**, *107*, 8816–8828.
- (62) Zapf, M.; Sidiropoulos, T.; Röder, R. Tailoring Spectral and Temporal Properties of Semiconductor Nanowire Lasers. *Advanced Optical Materials* **2019**, *7*, 1900504.
- (63) Alanis, J. A.; Chen, Q.; Lysevych, M.; Burgess, T.; Li, L.; Liu, Z.; Tan, H. H.; Jagdish, C.; Parkinson, P. Threshold reduction and yield improvement of semiconductor nanowire lasers: Via processing-related end-facet optimization. *Nanoscale Advances* **2019**, *1*, 4393–4397.

- (64) Gurioli, M.; Vinattieri, A.; Colocci, M.; Deparis, C.; Massies, J.; Neu, G.; Bosacchi, A.; Franchi, S. Temperature dependence of the radiative and nonradiative recombination time in GaAs/AlGaAs quantum-well structures. *Physical Review B* **1991**, *44*, 3115–3124.
- (65) Zawadzka, A.; Plóciennik, P.; Strzelecki, J. Temperature-dependent luminescence dynamics for ZnO thin films. *Optical and Quantum Electronics* **2014**, *46*, 87–101.
- (66) Brandt, O.; Ringling, J.; Ploog, K. H.; Wünsche, H.-J.; Henneberger, F. Temperature dependence of the radiative lifetime in GaN. *Physical Review B* **1998**, *58*, R15977–R15980.
- (67) Niemeyer, M.; Kleinschmidt, P.; Walker, A. W.; Mundt, L. E.; Timm, C.; Lang, R.; Hannappel, T.; Lackner, D. Measurement of the non-radiative minority recombination lifetime and the effective radiative recombination coefficient in GaAs. *AIP Advances* **2019**, *9*.
- (68) Keyes, B. M.; Dunlavy, D. J.; Ahrenkiel, R. K.; Shaw, G.; Summers, G. P.; Tzafaras, N.; Lentz, C. Time-resolved photoluminescence of undoped InP. *Journal of Applied Physics* **1994**, *75*, 4249–4251.
- (69) Li, H.; Kam, C.; Lam, Y.; Ji, W. Optical nonlinearities and photo-excited carrier lifetime in CdS at 532 nm. *Optics Communications* **2001**, *190*, 351–356.
- (70) Lami, J.-F.; Hirlimann, C. Two-photon excited room-temperature luminescence of CdS in the femtosecond regime. *Physical Review B* **1999**, *60*, 4763–4770.
- (71) Chichibu, S. F.; Shima, K.; Kojima, K.; Takashima, S.-y.; Ueno, K.; Edo, M.; Iguchi, H.; Narita, T.; Kataoka, K.; Ishibashi, S.; Uedono, A. Room temperature photoluminescence lifetime for the near-band-edge emission of epitaxial and ion-implanted GaN on GaN structures. *Japanese Journal of Applied Physics* **2019**, *58*, SC0802.

- (72) Jen, F.-Y.; Lu, Y.-C.; Chen, C.-Y.; Wang, H.-C.; Yang, C. C.; Zhang, B.-p.; Segawa, Y. Temperature-dependent exciton dynamics in a ZnO thin film. *Applied Physics Letters* **2005**, *87*.
- (73) Al-Abri, R.; Amairi, N. A.; Church, S.; Byrne, C.; Sivakumar, S.; Walton, A.; Magnusson, M. H.; Parkinson, P. Sub-Picosecond Carrier Dynamics Explored using Automated High-Throughput Studies of Doping Inhomogeneity within a Bayesian Framework. *Small* **2023**, *19*, 2300053.
- (74) Zhang, Y.; Davis, G.; Fonseka, H. A.; Velichko, A.; Gustafsson, A.; Godde, T.; Saxena, D.; Aagesen, M.; Parkinson, P. W.; Gott, J. A.; Huo, S.; Sanchez, A. M.; Mowbray, D. J.; Liu, H. Highly Strained III-V-V Coaxial Nanowire Quantum Wells with Strong Carrier Confinement. *ACS Nano* **2019**, *13*, 5931–5938.
- (75) Klingshirn, C.; Hauschild, R.; Fallert, J.; Kalt, H. Room-temperature stimulated emission of ZnO: Alternatives to excitonic lasing. *Physical Review B* **2007**, *75*, 115203.
- (76) Versteegh, M. A. M.; Vanmaekelbergh, D.; Dijkhuis, J. I. Room-Temperature Laser Emission of ZnO Nanowires Explained by Many-Body Theory. *Physical Review Letters* **2012**, *108*, 157402.

Supporting Information

The nanowires studied in this work were grown using various approaches that are summarized in this document. For high-throughput investigation, each sample of nanowires was suspended in IPA using ultrasonication for 5s, and transferred to quartz substrates using drop-casting.¹ These nanowires were then studied using a number of high-throughput experiments. The details of these experiments can be found in a previous publication.²

Nanowire growth details

InP

InP nanowires were grown using selective area epitaxy (SAE) with metal-organic chemical vapour deposition (MOCVD). A 150 nm thick SiO₂ mask was deposited on InP (111) wafers, followed by electron beam lithography and dry etching. This produced a mask with dimensions of 100 × 100 μm, which were placed in a close coupled showerhead MOCVD reactor, where trimethyl (TM) Indium and phosphine (PH₃) were used as precursors with molar flow rates of 6 × 10⁻⁶ and 4.91 × 10⁻⁴ mol min⁻¹, respectively. Nanowires were grown at 730 °C and base pressure of 100 mbar with H₂ as the carrier gas at a total flow rate of 14.5 L min⁻¹. More details can be found in reference.³

GaAs

GaAs nanowires were grown on (111) GaAs substrates using a vapor-liquid-solid (VLS) approach via MOCVD in a similar manner to those in ref.⁴ Au particles were used to catalyse the growth, which was achieved using TMGa, TMAI and arsine (AsH₃) precursors for Ga, Al and As respectively.

The growth process involved a two-temperature procedure for the GaAs core. Initially, a 1- minute nucleation step growth at 450 °C, followed by 45 minutes of growth at 375 °C.

Subsequently, the temperature was raised to 750 °C in an AsH₃ atmosphere, and an AlGaAs shell was grown for 0.5 minutes with a TMAI/(TMGa + TMAI) ratio of 0.5. Finally, a GaAs cap layer was deposited for 1.5 minutes at 750 °C to shield the AlGaAs shell from oxidation. More details can be found in reference.⁴

ZnGaAs

Zn doped GaAs nanowires were grown using a similar Au-catalysed VLS growth approach to the GaAs wires, on (111) GaAs substrates. In this case, the doping was achieved using diethylzinc (DEZn) as a precursor. A capping layer was not included: more information on these wires can be found in reference.¹

AlGaAs/GaAs

AlGaAs/GaAs quantum well nanowires were produced in a similar manner to the GaAs wires: this included a GaAs core which grown using a Au-catalyst mediated two-temperature VLS approach, and an AlGaAs shell layer. This was followed by 8 GaAs/AlGaAs quantum well and barrier layers using an established recipe provided in reference.⁵ These wires were also used in a previous optical study.⁶

GaAsP/GaAs

GaAsP/GaAs quantum well nanowires were grown using self-catalysed VLS growth in a molecular beam epitaxy (MBE) approach onto p-type (111) Si substrates. A GaAsP nanowire core was grown at a temperature of 640 °C for 90 minutes. The remaining Ga droplet was then consumed by saturating the growth with As and P flux. 3 GaAs/GaAsP quantum well/barrier shell layers were grown at 550 °C, followed by outer shell layers of AlGaAsP and GaAsP. Full details of the growth can be found in reference.⁷

CdS

CdS nanowires were grown using the VLS technique via CVD inside a horizontal-tube vacuum furnace. CdS powder was sublimated at temperatures of 800 °C and the vapor was transported by Ar carrier gas towards the growth substrates, which were kept at lower temperatures. The growth substrates (001-Si) were coated with a 10-15 nm Au layer, acting as a catalyst for the growth of CdS NWs, which was carried out for 30 minutes at temperatures between 720 and 600 °C. Further details on the growth of these CdS NWs can be found in reference.⁸

GaN

GaN nanowires were grown using a self-catalysed approach via MOCVD on c-plane sapphire substrates. The substrates were annealed in H₂ at a temperature of 1060 °C and then nitrided at 1080 using NH₃ gas. TMGa and NH₃ were used as precursor gases for a GaN nucleation layer, and nanowire growth was performed at a temperature of 750 °C, using silane (SiH₄) as an additional precursor to prevent lateral growth. Full growth details can be found in reference.⁹

ZnO

ZnO nanowires were grown via VLS in a similar manner to the CdS samples. In this case, a mixture of ZnO and graphite powder with molar ratio 1:1 was used as the precursor and was sublimated at a temperature of 1050 °C. The vapor was transported using Ar + O₂ as the carrier gas and the growth occurred at temperatures between 960 and 1150 °C. Further details on the growth of ZnO NWs are given in reference.¹⁰

References

- (1) Alanis, J. A.; Lysevych, M.; Burgess, T.; Saxena, D.; Mokkaapati, S.; Skalsky, S.; Tang, X.; Mitchell, P.; Walton, A. S.; Tan, H. H.; Jagadish, C.; Parkinson, P. Optical Study of p-Doping in GaAs Nanowires for Low-Threshold and High-Yield Lasing. *Nano Letters* **2019**, *19*, 362–368.
- (2) Church, S. A.; Choi, H.; Al-Amairi, N.; Al-Abri, R.; Sanders, E.; Oksenberg, E.; Joselevich, E.; Parkinson, P. W. Holistic Determination of Optoelectronic Properties using High-Throughput Spectroscopy of Surface-Guided CsPbBr₃ Nanowires. *ACS Nano* **2022**, *16*, 9086–9094.
- (3) Gao, Q.; Saxena, D.; Wang, F.; Fu, L.; Mokkaapati, S.; Guo, Y.; Li, L.; Wong-Leung, J.; Caroff, P.; Tan, H. H.; Jagadish, C. Selective-area epitaxy of pure wurtzite InP nanowires: High quantum efficiency and room-temperature lasing. *Nano Letters* **2014**, *14*, 5206–5211.
- (4) Saxena, D.; Mokkaapati, S.; Parkinson, P.; Jiang, N.; Gao, Q.; Tan, H. H.; Jagadish, C. Optically Pumped Room-Temperature GaAs Nanowire Lasers. *Nature Photonics* **2013**, *7*, 963–968.
- (5) Saxena, D.; Jiang, N.; Yuan, X.; Mokkaapati, S.; Guo, Y.; Tan, H. H.; Jagadish, C. Design and Room-Temperature Operation of GaAs/AlGaAs Multiple Quantum Well Nanowire Lasers. *Nano Letters* **2016**, *16*, 5080–5086.
- (6) Alanis, J. A.; Saxena, D.; Mokkaapati, S.; Jiang, N.; Peng, K.; Tang, X.; Fu, L.; Tan, H. H.; Jagadish, C.; Parkinson, P. Large-scale statistics for threshold optimization of optically pumped nanowire lasers. *Nano Letters* **2017**, *17*, 4860–4865.
- (7) Zhang, Y.; Davis, G.; Fonseka, H. A.; Velichko, A.; Gustafsson, A.; Godde, T.; Saxena, D.; Aagesen, M.; Parkinson, P. W.; Gott, J. A.; Huo, S.; Sanchez, A. M.; Mow-

- bray, D. J.; Liu, H. Highly Strained III–V–V Coaxial Nanowire Quantum Wells with Strong Carrier Confinement. *ACS Nano* **2019**, *13*, 5931–5938.
- (8) Geburt, S.; Thielmann, A.; Röder, R.; Borschel, C.; McDonnell, A.; Kozlik, M.; Kühnel, J.; Sunter, K. A.; Capasso, F.; Ronning, C. Low threshold room-temperature lasing of CdS nanowires. *Nanotechnology* **2012**, *23*, 365204.
- (9) Nian Jiang,; Saptarsi Ghosh,; Martin Frentrup,; M. Fairclough, S.; Kagiso Loeto,; Gunnar Kusch,; A. Oliver, R.; J. Joyce, H. Complications in silane-assisted GaN nanowire growth. *Nanoscale Advances* **2023**, *5*, 2610–2620.
- (10) Borchers, C.; Müller, S.; Stichtenoth, D.; Schwen, D.; Ronning, C. Catalyst-Nanostructure Interaction in the Growth of 1-D ZnO Nanostructures. *The Journal of Physical Chemistry B* **2006**, *110*, 1656–1660.